J. Fluid Mech. (2007), *vol.* 586, *pp.* 59–81.
doi:10.1017/S0022112007007240 Printed in the United Kingdom

Reynolds-number dependence of line and surface stretching in turbulence: folding effects

SUSUMU GOTO AND SHIGEO KIDA

Department of Mechanical Engineering and Science, Kyoto University,
Yoshida-Honmachi, Sakyo, Kyoto, 606-8501, Japan

(Received 30 November 2005 and in revised form 13 January 2007)

The stretching rate, normalized by the reciprocal of the Kolmogorov time, of sufficiently extended material lines and surfaces in statistically stationary homogeneous isotropic turbulence depends on the Reynolds number, in contrast to the conventional picture that the statistics of material object deformation are determined solely by the Kolmogorov-scale eddies. This Reynolds-number dependence of the stretching rate of sufficiently extended material objects is numerically verified both in two- and three-dimensional turbulence, although the normalized stretching rate of infinitesimal material objects is confirmed to be independent of the Reynolds number. These numerical results can be understood from the following three facts. First, the exponentially rapid stretching brings about rapid multiple folding of finite-sized material objects, but no folding takes place for infinitesimal objects. Secondly, since the local degree of folding is positively correlated with the local stretching rate and it is non-uniformly distributed over finite-sized objects, the folding enhances the stretching rate of the finite-sized objects. Thirdly, the stretching of infinitesimal fractions of material objects is governed by the Kolmogorov-scale eddies, whereas the folding of a finite-sized material object is governed by all eddies smaller than the spatial extent of the objects. In other words, the time scale of stretching of infinitesimal fractions of material objects is proportional to the Kolmogorov time, whereas that of folding of sufficiently extended material objects can be as long as the turnover time of the largest eddies. The combination of the short time scale of stretching of infinitesimal fractions and the long time scale of folding of the whole object yields the Reynolds-number dependence. Movies are available with the online version of the paper.

1. Introduction

Marbling (see the visualization in figure 6) stems from a successive combination of stretching and folding of the boundary between two materials. We fluid mechanists desire to understand and control the stretching and folding because the pattern is not only beautiful but closely related to the mixing of two materials, and because the mixing is a crucial function of fluid flow, especially of turbulence.

A material object is defined as one which always consists of the same set of fluid particles (Batchelor 1952). Therefore, a material line in two-dimensional flow or a surface in three-dimensional flow constitutes a boundary between two regions of the fluid. In other words, the line or surface can be regarded as the boundary between two liquid materials if they have same density, and molecular diffusion is negligible compared to the advection effects. It is, therefore, useful to study deformation of material lines and surfaces to understand the mechanism and statistics of turbulent

mixing. The stretching of material objects in turbulence has been studied intensively by many authors (Batchelor 1952; Cocke 1969; Girimaji & Pope 1990; Huang 1996; Kida & Goto 2002; Goto & Kida 2002, 2003; Guala *et al.* 2005). Their exponentially rapid stretching was predicted by Batchelor (1952) and verified numerically by Girimaji & Pope (1990). The folding of material objects, however, has not been studied so far because the properties of folding of material objects cannot be captured easily even in numerical turbulence; for this purpose, finite-sized material objects must be tracked for a sufficiently long time. Since material objects are stretched exponentially in time, this kind of simulation requires huge computational resources.

The conventional idea of deformation of material objects is that the stretching is described solely by the characteristics of the smallest-scale (i.e. the Kolmogorov length) eddies in isotropic turbulence. Such eddies, having the smallest time scale, make a dominant contribution to the stretching of material objects, and this is the origin of the exponential stretching. But intensive folding of material objects is brought about by eddies of all scales (see figure 12, below) which affects the mean value of the stretching rate as the statistical weight. The purpose of the present article is to clarify how the folding leads to the Reynolds-number dependence of the mean stretching rate.

Note that this effect of folding on the mean stretching rate cannot be observed in moderate-Reynolds-number flows because it is the multi-scale nature of turbulence that plays a crucial role. Therefore, in addition to three-dimensional turbulence at relatively large Reynolds numbers, we conduct numerical simulations of two-dimensional turbulence, in which a sufficiently wide inertial range can be realized. Note also that the Reynolds-number dependence of the stretching rate cannot be investigated by the simulation of fixed-length material lines, or of infinitesimal line or surface elements. The mean stretching rate (about $0.17\tau_\eta^{-1}$) of fixed-length material lines (Goto & Kida 2003) and that (about $0.13\tau_\eta^{-1}$) of infinitesimal line elements (Girimaji & Pope 1990) are independent of the Reynolds number. Here τ_η is the Kolmogorov time. These results seem to contrast with the conclusion of the present article that the mean stretching rate of sufficiently extended material objects depends on the Reynolds number in a non-trivial manner. This superficial contradiction is solved by taking folding effects into account. The folding of material objects has been completely ignored in those simulations of fixed-length lines and of infinitesimal material elements.

The rest of the article is organized as follows. The next section briefly outlines our direct numerical simulations (DNS) of material lines and surfaces both in two-dimensional and three-dimensional turbulence. We report, in § 3, the numerical evidence of the Reynolds-number dependence of the stretching rate of sufficiently extended material objects. In the discussion of this, it is crucial to introduce the spatial extent of material objects because their folding features (and therefore their mean stretching rate) are different depending on the extent. The physical explanation of this interesting numerical result is given in § 4. Concluding remarks are given in the last section.

2. Direct numerical simulation

2.1. *Material lines and surfaces*

A material line is expressed numerically by a chain of short line segments. Since the line length increases rapidly in time, we employ an interpolation along the line at every numerical time step to make each segment always shorter than a threshold of the order of the Kolmogorov length η. The line length becomes longer in time, and so

the number of segments increases. Therefore, the computer memory limits the total simulation time. A material surface, on the other hand, is constructed by a set of small triangles. Similarly to material lines, we monitor the side length of each triangle. If it is longer than a threshold of $O(\eta)$ a triangle is divided into two. We store all the connections between triangles as well as their position vectors to carry out the divisions of triangles efficiently.

Here, we discuss the choice of threshold for the interpolation of material objects. For infinitesimal line elements, in Kida & Goto (2002) we have checked the relevance of the simulated statistics of stretching by changing the threshold, and concluded that they are independent of the threshold if it is as small as η. This is expected to be valid also for the finite-sized objects because the interpolation is concerned with the length scale parallel to the objects, though the length scale (e.g. the width between streaks observed in figure 6) perpendicular to them can be much shorter than η. It is shown below that the Reynolds-number dependence of the stretching rate of finite-sized objects can be explained without taking account of the action of sub-Kolmogorov-scale flow structures. Nevertheless, we cannot fully exclude the possibility that such structures may affect the statistics of material objects, since some references (e.g. Frisch & Vergassola 1991; Yakhot & Sreenivasan 2005) have reported Reynolds-number dependence in the intermediate dissipation range.

By the definition of a material object, the position vector $\boldsymbol{x}_p(t)$ of any point in it moves according to the advection equation,

$$\frac{\mathrm{d}}{\mathrm{d}t}\boldsymbol{x}_p = \boldsymbol{u}(\boldsymbol{x}_p(t), t), \tag{2.1}$$

where $\boldsymbol{u}(\boldsymbol{x}, t)$ is a velocity field. The characteristics of the present numerical turbulence is described in the following two subsections. Equation (2.1) is integrated numerically using the fourth-order Runge–Kutta scheme. The right-hand side of (2.1) is estimated by the third-order Lagrangian interpolation of the velocity field at numerical grids. The temporal evolution of the velocity field is simulated simultaneously with that of material objects.

2.2. *Lines and surfaces in three-dimensional turbulence*

In this subsection we describe three-dimensional DNS. Statistically stationary homogeneous isotropic turbulence of an incompressible fluid is realized by solving the Navier–Stokes equation with an external force $\boldsymbol{f}$,

$$\left(\frac{\partial}{\partial t} + \boldsymbol{u}\cdot\nabla\right)\boldsymbol{u} = -\frac{1}{\rho}\nabla p + \nu\nabla^2\boldsymbol{u} + \boldsymbol{f}, \tag{2.2}$$

and the continuity equation $\nabla\cdot\boldsymbol{u} = 0$, under the periodic boundary condition of period 2π in three orthogonal directions. Here, $p(\boldsymbol{x}, t)$, ρ and ν are the pressure, the constant density and the kinematic viscosity of the fluid. We integrate (2.2) numerically by the fourth-order Runge–Kutta scheme, where the spatial derivative is estimated by a de-aliased Fourier spectral method. The large-scale external forcing is implemented by fixing the amplitudes of Fourier components in a low-wavenumber region (say $k < \sqrt{8}$). Numerical parameters are given in Goto & Kida (2003). We simulate turbulence at five different Reynolds numbers,

$$R_\lambda = \sqrt{\frac{20}{3\nu\epsilon}}\mathscr{E}, \tag{2.3}$$

(*a*)		IIIA	IIIB	IIIC	IIID	IIIE
	N^3	128^3	128^3	256^3	512^3	512^3
	$\mathscr{E}$	0.544	0.573	0.586	0.585	0.601
	ϵ	0.124	0.127	0.124	0.119	0.121
	$\mathscr{T}$	4.39	4.51	4.73	4.92	4.97
	τ_η	2.02×10^{-1}	1.41×10^{-1}	1.01×10^{-1}	7.26×10^{-2}	5.09×10^{-2}
	$\mathscr{L}$	3.23	3.42	3.62	3.76	3.85
	η	3.17×10^{-2}	1.87×10^{-2}	1.12×10^{-2}	6.74×10^{-3}	3.99×10^{-3}
	$k_{\max}\eta$	1.91	1.12	1.35	1.62	0.96
	R_λ	5.65×10	8.31×10	1.21×10^2	1.75×10^2	2.52×10^2

(*b*)		IIA	IIB	IIC	IID
	N^2	512^2	1024^2	2048^2	4096^2
	$\mathscr{E}$	10	6.3	3.6	1.7
	ϵ	3.0	1.4	0.60	0.20
	$\mathscr{L}$	0.38	0.32	0.29	0.23
	η	6.1×10^{-2}	3.1×10^{-2}	1.5×10^{-2}	7.7×10^{-3}
	$\mathscr{T}$	0.12	0.13	0.15	0.17
	τ_η	1.2×10^{-2}	9.6×10^{-3}	7.9×10^{-3}	6.8×10^{-3}
	$\mathscr{L}/\eta$	6.3	10	19	30
	$\mathscr{T}/\tau_\eta$	10	13	19	25

TABLE 1. Statistics of simulated (*a*) three-dimensional turbulence and (*b*) two-dimensional turbulence.

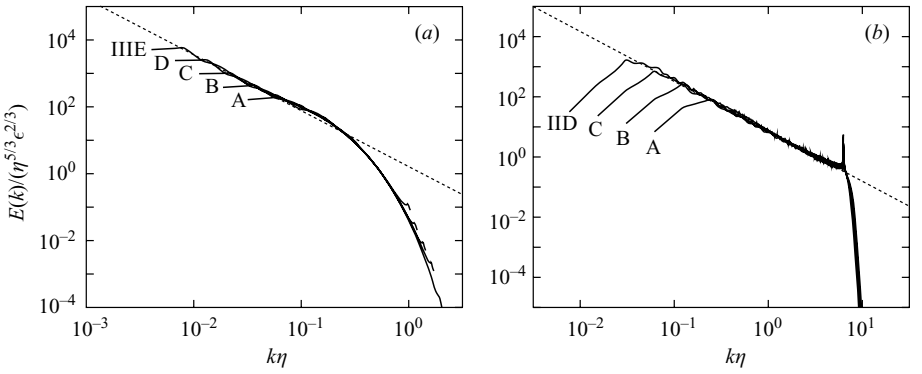

FIGURE 1. Energy spectra $E(k)$ normalized by the Kolmogorov length η and the energy dissipation rate ϵ: (*a*) three-dimensional DNS, (*b*) two-dimensional DNS. Dashed lines indicate the Kolmogorov inertial-range spectrum proportional to $k^{-5/3}$. See table 1 for the statistics of simulated flow in the respective cases.

based on the Taylor length, by changing ν and the number N^3 of numerical grid points. Here, $\mathscr{E}$ and ϵ are the mean energy per unit mass and its dissipation rate per unit time, respectively. The statistics of the simulated velocity field are summarized in table 1(*a*). The largest and the smallest length scales are defined by $\mathscr{L} \equiv \mathscr{E}^{3/2}/\epsilon$ and $\eta \equiv \epsilon^{-1/4}\nu^{3/4}$, respectively. Correspondingly, the largest and the smallest time scales are defined by $\mathscr{T} \equiv \mathscr{E}/\epsilon$ and $\tau_\eta \equiv \epsilon^{-1/2}\nu^{1/2}$, respectively. The simulated energy spectra $E(k)$, normalized by the Kolmogorov variables, are plotted in figure 1(*a*). Only a narrow inertial range, where the energy spectrum takes the $k^{-5/3}$ power form, is observed even at the highest Reynolds number ($R_\lambda = 250$).

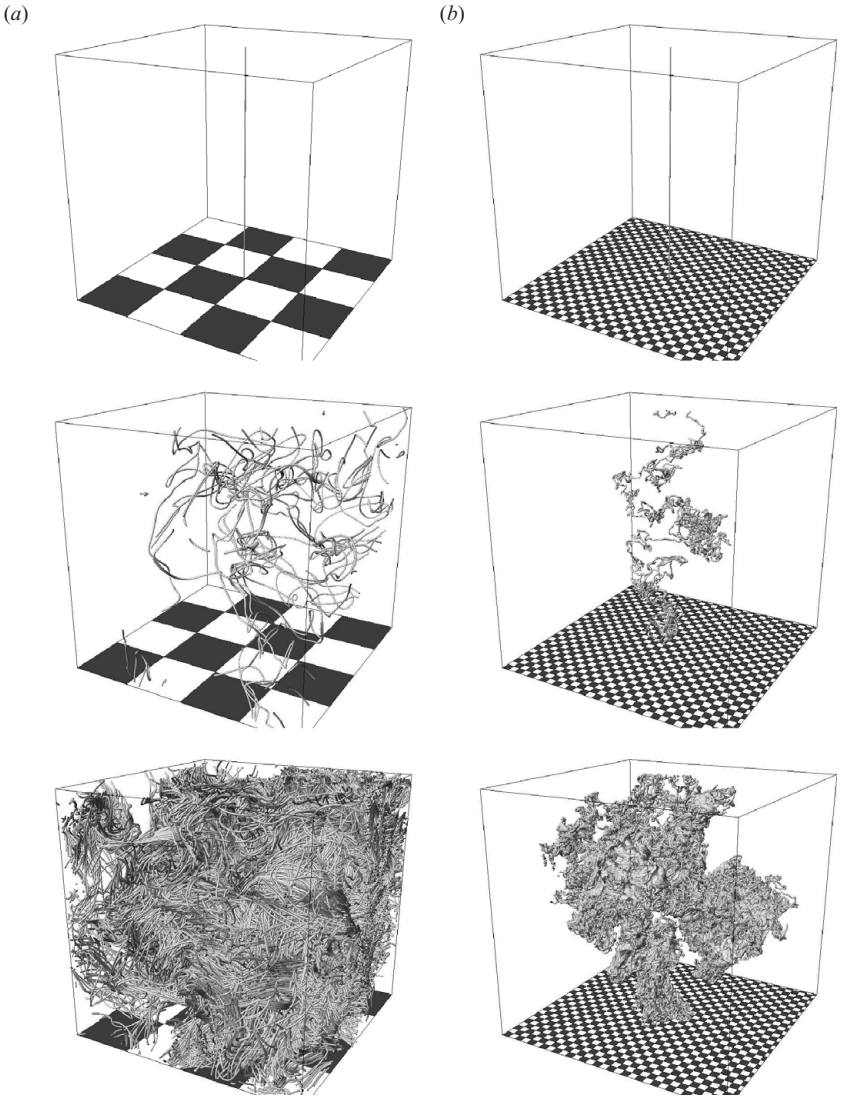

FIGURE 2. Temporal evolution of a line in three-dimensional turbulence. $t = 0$ (top), $25\tau_\eta$ (middle) and $50\tau_\eta$ (bottom). The entire simulation box (side is about $2\mathscr{L}$) is shown, and the line is cropped by the box. The bottom chessboard pattern indicates squares of side length 50η. (*a*) Run IIIA. (*b*) IIIE.

In figure 2 we plot the typical temporal evolution of a line for two different Reynolds numbers $R_\lambda = 57$ and 250. The time increment between successive panels is $25\tau_\eta$. The entire simulation box is presented, whose side length is about $2\mathscr{L}$ irrespective of the Reynolds number. The chessboard pattern on the bottom indicates the length of 50η. Two interesting characteristic features may be recognized in this figure. The first is the characteristic length of deformations, if measured in units of $\mathscr{L}$, is a decreasing function of R_λ. Note, however, that as already demonstrated in figure 2 of Goto & Kida (2003), it is hardly dependent on R_λ if viewed on the Kolmogorov scale, i.e. the size of the chessboard pattern. This is consistent with Batchelor's (1952) idea that the deformation of material objects is due to the Kolmogorov-scale eddies.

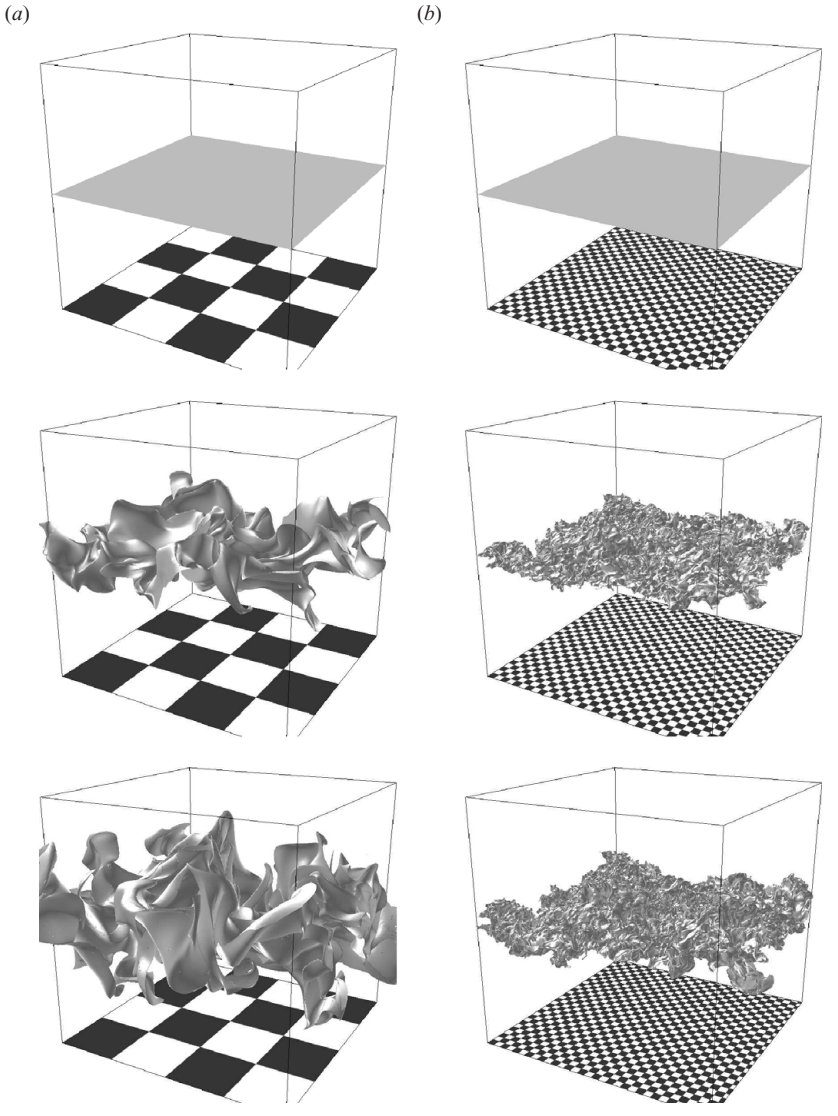

FIGURE 3. Temporal evolution of a surface in three-dimensional turbulence. $t = 0$ (top), $5\tau_\eta$ (middle) and $10\tau_\eta$ (bottom). Entire simulation box (side is about $2\mathscr{L}$) is shown. The bottom chessboard pattern indicates 50η squares. (*a*) Run IIIA. (*b*) IIIE. A movie of (*a*) is available with the online version of the paper (movie 1).

Note, in passing that the mean curvature of fixed-length material lines is about $0.1\eta^{-1}$ irrespective of the Reynolds number (Goto & Kida 2003). Here, the mean curvature is estimated by the average of local curvatures of short fractions of finite-length lines with the statistical weight proportional to the length of each fraction. The second characteristic feature is that the extent of the deformed material objects is narrower for the larger Reynolds number in units of $\mathscr{L}$. This may imply that for larger Reynolds numbers material lines are confined in smaller regions. It is this intensive accumulation and pile-up of material lines that affects the Reynolds-number dependence of the statistics of material object stretching.

A similar Reynolds-number dependence is observed in the deformation of material surfaces as shown in figure 3. Here, the temporal evolution of a material surface,

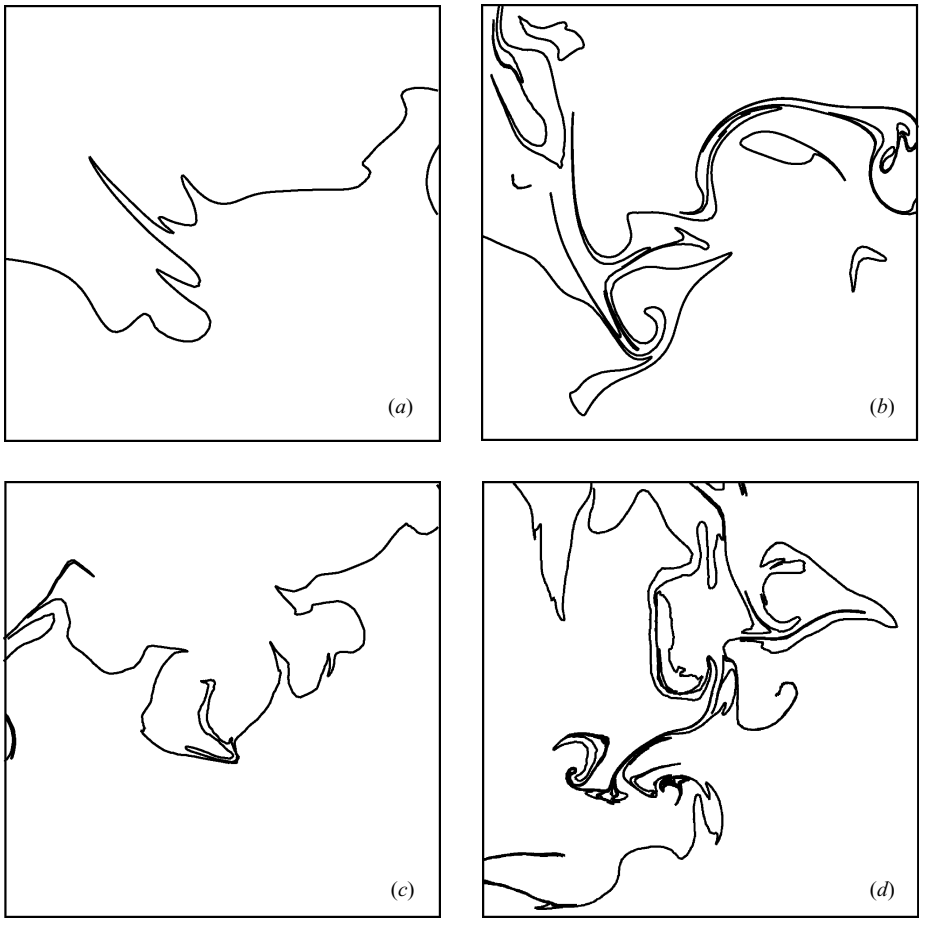

FIGURE 4. Cross-sections of a material surface in three-dimensional turbulence. Side length of a square is 100η. (a, b) Run IIIA; (c, d) IIID. (a, c) $t = 5\tau_\eta$; (b, d) $10\tau_\eta$.

which starts with a flat plane, is drawn in the entire simulation box at times $5\tau_\eta$ and $10\tau_\eta$ for two Reynolds numbers $R_\lambda = 57$ and 250 in (a) and (b), respectively. The size of the chessboard pattern is the same as in figure 2. It is seen, on this integral scale $\mathscr{L}$, that the vertical extent of the surface is narrower and the deformation is finer for the larger Reynolds number. On the Kolmogorov scale, on the other hand, the degree of deformation is comparable for the two Reynolds numbers. This is clearly seen in figure 4, where we draw the cross-sections of surfaces sliced through an arbitrary plane in a square of side length 100η at $t = 5\tau_\eta$ and $10\tau_\eta$ for $R_\lambda = (a, b)$ 57 and (c, d) 250. Some important characteristic features may be recognized by comparing these four cross-sections. First, the curvature of the lines is nearly the same in magnitude irrespective of the elapsed time and the Reynolds number. In fact, the radius of curvature is of $O(10\eta)$, which is comparable with the mean diameter of the smallest-scale eddies (Goto & Kida 2003). Secondly, the lines are not simple but multiple in many places, which represents the multiple layers of material surfaces. The multiplicity is stronger for the larger Reynolds number and is enhanced more and more as time progresses. Thirdly, although much deformed, the T-shaped form of various sizes is embedded at many places along the multiple lines. This T-shaped form is generated by swirling flows induced by pairs of anti-parallel vortices (see Goto & Kida 2003).

2.3. *Lines in two-dimensional turbulence*

It will become clear below that the stretching of material objects is not only a Kolmogorov-scale phenomenon, but also eddies of various length scales play roles in the statistics of the stretching rate. In other words, the mean stretching rate cannot be determined by dissipation-range properties only. This is the reason why we conduct two-dimensional DNS, where we can simulate a wider inertial range by using a smaller number of grid points compared to three-dimensional DNS. We can also partly circumvent, in this two-dimensional case, the exponential growth of computational memory requirement by employing a merger technique; that is, when any two of line segments approach to within some close distance they are identified, and thereafter only one of them is tracked as the representative of the two. Even though we have to estimate the sum of merged segment lengths, this leads to a huge saving of computational resources. We use this merger technique in later sections to estimate the line statistics in two-dimensional DNS. In the three-dimensional case, however, it is not numerically straightforward to use this kind of technique.

Similarly to the three-dimensional DNS, we integrate the two-dimensional version of the Navier–Stokes equation (2.2) numerically by employing the fourth-order Runge–Kutta scheme and the Fourier spectrum method. Since the energy is cascaded up to larger scales, unlike three-dimensional turbulence, we excite the flow at small scales. In practice, we keep the magnitudes of Fourier components in a high-wavenumber region around $k = k_f$ constant in time. Then, the forcing scale $2\pi/k_f$ gives the lower length limit of the inertial range so that we may call it the Kolmogorov scale and denote it by $\eta \equiv 2\pi/k_f$. In order to compress the enstrophy-cascade-and-dissipation range (i.e. $k > k_f$), we replace the viscous term $\nu\nabla^2\boldsymbol{u}$ in (2.2) by a hyper-viscous term $-\nu'\nabla^{16}\boldsymbol{u}$. In addition, we introduce a hyper-drag term $D\nabla^{-2}\boldsymbol{u}$ into this equation to avoid energy accumulation at the largest scales. The details of numerics of this two-dimensional turbulence are described in Goto & Vassilicos (2004). We simulate four different turbulence states by using different forcing scales and numbers N^2 of grid points. The scale ratio $\mathscr{L}/\eta$ is used as an index of the degree of turbulence development, instead of the Reynolds number R_λ in three-dimensional turbulence; recall the proportionality $R_\lambda \sim (\mathscr{L}/\eta)^{2/3}$ in three-dimensional isotropic turbulence. We list the statistics of the simulated velocity fields in table 1(*b*) where the Kolmogorov time τ_η is estimated by the reciprocal of the r.m.s. vorticity, ϵ by the constant energy flux in the inertial range (see figure 2 of Goto & Vassilicos 2004), and $\mathscr{L}$ by the integral length scale of the second-order longitudinal velocity correlation function. The energy spectra shown in figure 1(*b*) exhibit a well-defined $k^{-5/3}$ power law developed through the inverse energy cascade (Kraichnan 1967; Leith 1968; Batchelor 1969).

In figure 5 we show the temporal evolution of a material line (identified as the boundary between the black and white regions) in a square of side length $10\mathscr{L}$ at $t = 0$, $5\tau_\eta$ and $10\tau_\eta$ for two different Reynolds numbers $\mathscr{L}/\eta =$ (*a*) 6.3 and (*b*) 30. A square of side length 10η is shown in each figure in order to indicate the domain size of figures 6 and 7 below. Similarly to the lines and surfaces in three-dimensional turbulence (figures 2 and 3) we observe, at the largest characteristic scale $\mathscr{L}$ of the turbulence, that the deformation of lines is finer in structure and narrower in extent for the larger Reynolds number. If, on the other hand, we magnify them to show a box of size 10η, the smallest scales of the flow, then the typical length of deformations appear comparable to each other (figure 6). This observation is also consistent with the conventional picture that material objects are deformed predominantly by the smallest-scale eddies. Indeed, by plotting the deformed material lines together with vorticity magnitude, we see a strong spatial correlation between the vortices and the

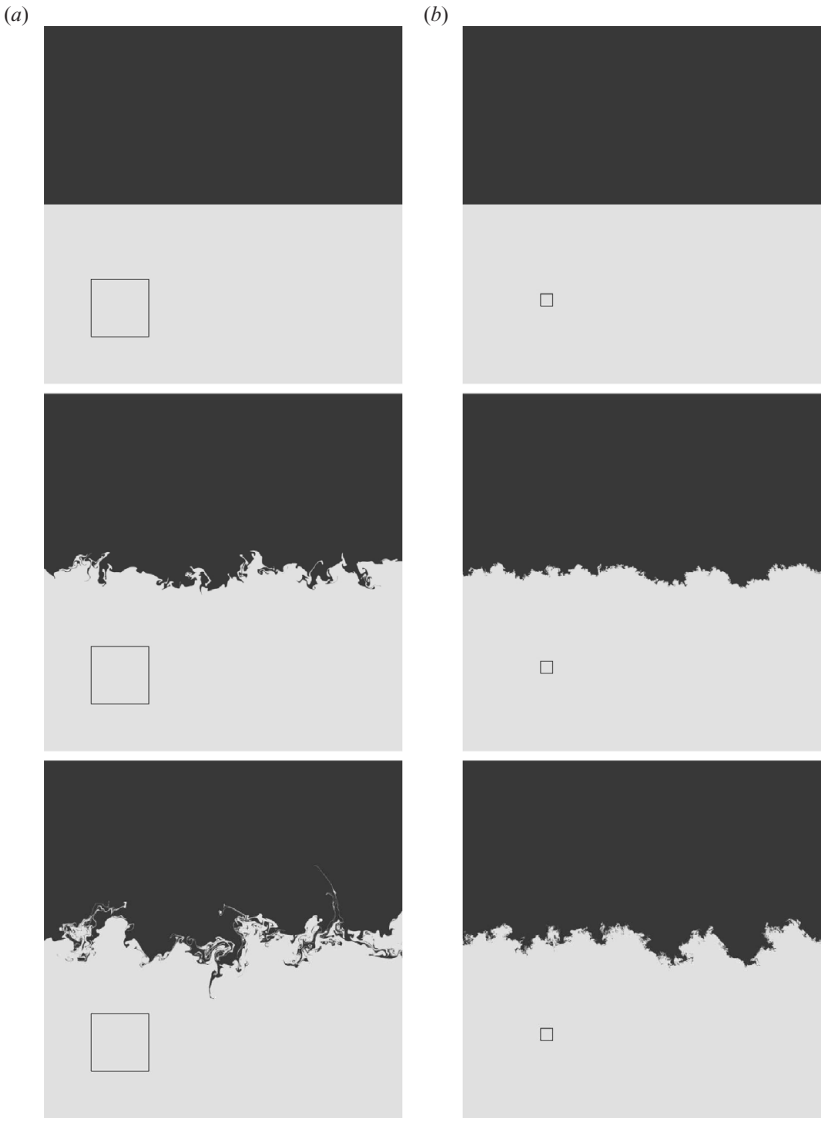

FIGURE 5. Temporal evolution of a material line in two-dimensional turbulence. $t = 0$ (top), $5\tau_\eta$ (middle) and $10\tau_\eta$ (bottom). The side length of each panel is equal to $10\mathscr{L}$, and that of the inset box is 10η. (*a*) Run IIA. (*b*) IID.

lines (figure 7). Almost all deformations of the line are caused by swirling motion induced by the smallest-scale vortices, and typical T-shaped forms are generated by pairs of anti-rotating vortices. However, it is important to notice here that the lines are not simple but folded many times and that the multiplicity is stronger for the larger Reynolds number and is enhanced more as the time elapses. As seen in the previous subsection, this behaviour of folding of lines in two-dimensional turbulence is the same as that of surfaces in three-dimensional turbulence (see figure 4). This is the key to understanding the Reynolds-number dependence of the stretching rate of material objects, as will be shown in the following sections.

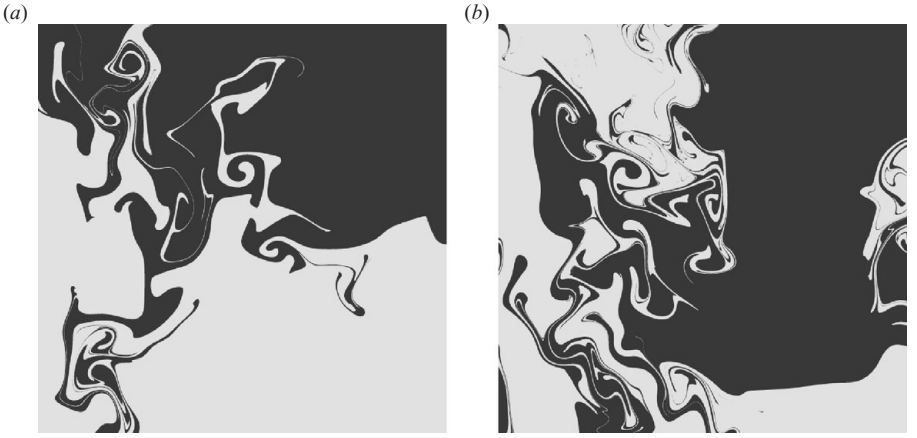

FIGURE 6. Magnification of figure 5 ($t = 10\tau_\eta$). The box size shown is 10η. (*a*) Run IIA. (*b*) IID.

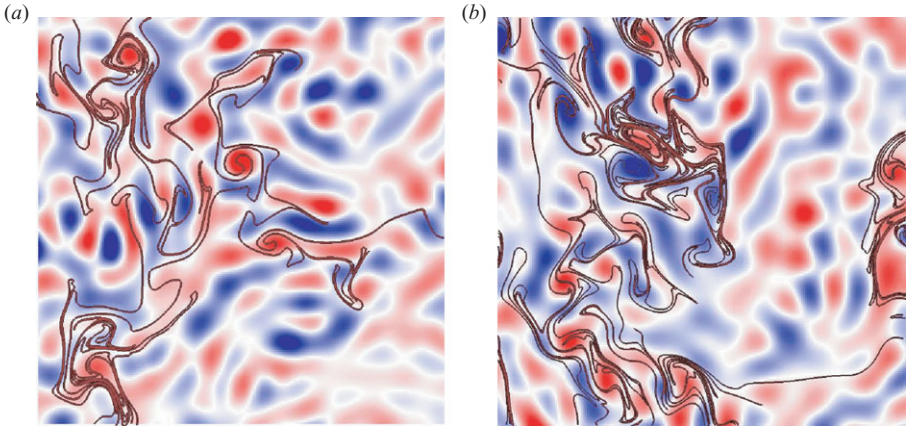

FIGURE 7. Same as figure 6 but also showing the contour of vorticity magnitude. Red and blue regions correspond respectively to positive and negative vorticity. Movies of (*a*) are available with the online version of the paper (movies 2 and 3).

3. Reynolds-number dependence of stretching rate

3.1. *Stretching rate and spatial extent*

The stretching rates of a material line of length $L(t)$ and a surface of area $A(t)$ are defined respectively by

$$\Gamma_\Delta \equiv \frac{\mathrm{d}}{\mathrm{d}t}\log L \qquad \text{and} \qquad \Gamma_\Delta \equiv \frac{\mathrm{d}}{\mathrm{d}t}\log A. \tag{3.1}$$

From these definitions, a constant stretching rate implies the exponential growth of $L(t)$ or $A(t)$. As will be seen below, the stretching rate $\Gamma_\Delta(t)$ of a material line depends on its spatial extent

$$\Delta \equiv \sqrt{\frac{1}{L}\int_L (\boldsymbol{x}(s) - \boldsymbol{x}_G)^2\,\mathrm{d}s}, \tag{3.2}$$

and the subscript Δ on Γ is a reminder. Here, s denotes the arclength along a line and

$$\boldsymbol{x}_G = \frac{1}{L}\int_L \boldsymbol{x}(s)\,\mathrm{d}s \tag{3.3}$$

is the centre of gravity of the line. Likewise, the stretching rate of a material surface depends on its extent, which may be defined in a similar manner to (3.2).

It is probable that the statistics of material objects are different depending on their initial shape. Keeping this in mind, hereafter we restrict considerations to the cases of initially straight lines and initially flat square surfaces.

3.2. *Infinitely extended line and surface*

We consider first the case that both of $L(t)$ and $\Delta(t)$ of a line are much longer than the integral length $\mathscr{L}$ of turbulence from the beginning. Since the spatial correlation of the turbulent velocity field is limited by $\mathscr{L}$, we expect that the stretching rate of such sufficiently extended lines is well-defined, that is, the fluctuation may be negligible. Let us denote this value by $\Gamma_\infty(t)$, i.e.

$$\Gamma_\infty \equiv \lim_{\Delta/\mathscr{L}\to\infty} \Gamma_\Delta, \tag{3.4}$$

which is the target quantity in the present subsection. We divide the line arbitrarily into M shorter lines whose lengths and extents at time t are denoted by $\ell^{(i)}(t)$ and $\delta^{(i)}(t)$, respectively. Here, $i = 1, \ldots, M$, and M is a positive integer. Then, length $L(t)$ is expressed by

$$L = \sum_{i=1}^{M} \ell^{(i)}, \tag{3.5}$$

and stretching rate $\Gamma_\infty(t)$ by

$$\Gamma_\infty = \sum_{i=1}^{M} \gamma^{(i)}\ell^{(i)} \Bigg/ \sum_{i=1}^{M} \ell^{(i)} = \frac{\langle \gamma\ell\rangle}{\langle\ell\rangle} (\equiv \langle\!\langle\gamma\rangle\!\rangle). \tag{3.6}$$

Here, $\gamma^{(i)} \equiv \mathrm{d}\log\ell^{(i)}/\mathrm{d}t$ is the stretching rate of the ith shorter line,

$$\langle f\rangle \equiv \sum_{i=1}^{M} f^{(i)} \tag{3.7}$$

denotes the arithmetic (non-weighted) average over M lines and double brackets $\langle\!\langle f\rangle\!\rangle \equiv \langle f\ell\rangle / \langle\ell\rangle$ stand for the weighted (by line length ℓ) average. Formula (3.6) indicates that the stretching rate $\Gamma_\infty(t)$ of a sufficiently extended line is expressed by the weighted average $\langle\!\langle\gamma\rangle\!\rangle$ of the stretching rates of the constitnent shorter lines, and more importantly that $\langle\!\langle\gamma\rangle\!\rangle$ is independent of the way the line was initially divided (i.e. the number M or the initial length $\ell^{(i)}(0)$). This is verified numerically in the next subsection (figure 8).

It should be emphasized here that since $\ell^{(i)}(t)$ is expressed by the time integral of $\gamma^{(i)}(t)$ as

$$\ell^{(i)}(t) = \ell^{(i)}(0)\exp\left[\int_0^t \gamma^{(i)}(t')\,\mathrm{d}t'\right], \tag{3.8}$$

$\gamma^{(i)}(t)$ and $\ell^{(i)}(t)$ must be positively correlated. Because the stretching of a material line is regarded as a multiplicative Markovian process, this positive correlation never

vanishes even in the infinite time limit (Goto & Kida 2002). Hence,

$$\Gamma_\infty = \langle\langle \gamma \rangle\rangle > \langle \gamma \rangle \tag{3.9}$$

because

$$\langle \gamma \ell \rangle > \langle \gamma \rangle \langle \ell \rangle. \tag{3.10}$$

Note, in passing, that the fact that $\langle \gamma \rangle$ and $\langle\langle \gamma \rangle\rangle$ give different values implies that $\langle \log \ell \rangle$ and $\log \langle \ell \rangle$ are different from each other because of the identities

$$\langle \gamma \rangle = \frac{\mathrm{d}}{\mathrm{d}t} \langle \log \ell \rangle \tag{3.11}$$

and

$$\langle\langle \gamma \rangle\rangle = \frac{\mathrm{d}}{\mathrm{d}t} \log \langle \ell \rangle. \tag{3.12}$$

Then, a general inequality $\langle \log \ell \rangle < \log \langle \ell \rangle$ (Childress & Gilbert 1995) leads to (3.9). Furthermore, the Reynolds-number dependence (or independence) of $\langle\langle \gamma \rangle\rangle$ (or $\langle \gamma \rangle$), which is shown below (figures 10, 11, 16 and 17), may be understood from the fact that the evolution of ℓ (or $\log \ell$) is a multiplicative (or an additive) Markovian process. Note that, owing to the exponential function in (3.8), ℓ (or $\log \ell$) is expressed by a product (or summation) of random variables, and that extreme events do (or do not) influence the entire statistics in a multiplicative (or additive) process.

In practice in our DNS, M_1 lines which are distributed randomly at $t = 0$ with length $\ell(0)$ are tracked, and such a simulation is repeated M_2 times. Then, the statistical homogeneity, isotropy and stationarity may permit us to calculate two averages $\langle \gamma \rangle$ and $\langle\langle \gamma \rangle\rangle$ over all the $M = M_1 M_2$ tracked lines, and to estimate the stretching rate $\Gamma_\infty(t)$ of sufficiently extended lines by

$$\Gamma_\infty = \lim_{M \to \infty} \frac{\langle \gamma \ell \rangle}{\langle \ell \rangle} = \lim_{M \to \infty} \langle\langle \gamma \rangle\rangle. \tag{3.13}$$

An argument can be made for material surfaces similar to the above for lines.

3.3. *Numerical results*

First, we confirm that the stretching rate $\Gamma_\infty(t)$, being calculated numerically by (3.13), is well-defined irrespective of the initial length of constitutive lines. We perform DNS of material lines in two dimensions with three different initial lengths (η, 10η and 100η) for four different Reynolds numbers listed in table 1(*b*). The initial positions and orientations of the lines tracked are chosen randomly. By using a sufficiently large number of lines (1000, 100 and 10 for $\ell(0) = \eta$, 10η and 100η, respectively) and realizations (8 (IIA), 8 (IIB), 4 (IIC) and 4 (IID)), we estimate $\langle\langle \gamma \rangle\rangle$, which is plotted in figure 8. It is clear that the weighted average $\langle\langle \gamma \rangle\rangle$ is independent of the initial length $\ell(0)$ of constitutive lines. This result confirms that the stretching rate $\Gamma_\infty(t)$ of sufficiently extended lines is defined well by (3.13).

Next, in figure 9, we compare the weighted average $\langle\langle \gamma \rangle\rangle$ of the stretching rate, which is independent of the initial line length $\ell(0)$, to the non-weighted average $\langle \gamma \rangle$ for three different $\ell(0)$. It is seen that the non-weighted average $\langle \gamma \rangle$ approaches the weighted average $\langle\langle \gamma \rangle\rangle$ as the initial length $\ell(0)$, and therefore the initial extent $\delta(0)$, increases. This is because in such a case where the mean spatial extent $\langle \delta \rangle$ of constitutive lines is sufficiently larger than $\mathscr{L}$, the fluctuation of γ is negligible and the right-hand side of (3.13) is approximated well by $\langle \gamma \rangle$. Thus,

$$\langle \gamma \rangle \to \Gamma_\infty = \langle\langle \gamma \rangle\rangle \quad \text{as} \quad \langle \delta \rangle / \mathscr{L} \to \infty. \tag{3.14}$$

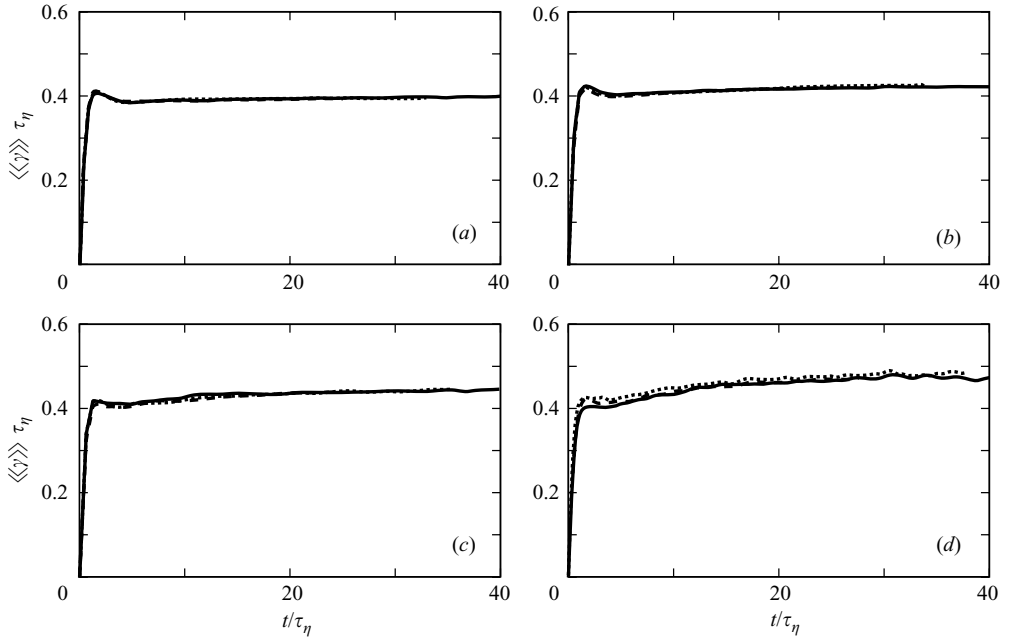

FIGURE 8. Weighted average of line stretching rate for three different initial lengths $\ell(0)$: dashed curves, $\ell(0)=\eta$; dotted curves, 10η; solid curves, 100η. (*a*) Run IIA. (*b*) IIB. (*c*) IIC. (*d*) IID.

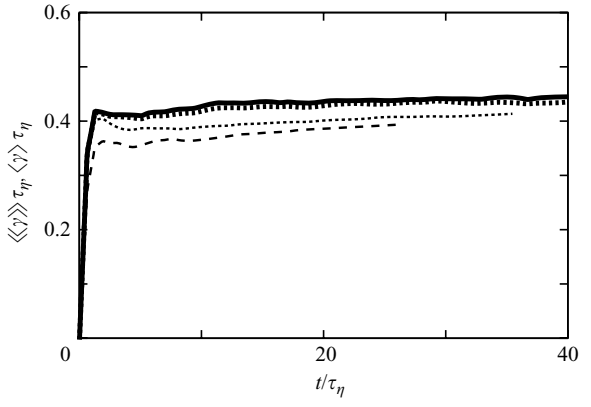

FIGURE 9. Comparison between the weighted $\langle\langle\gamma\rangle\rangle$ and non-weighted averages $\langle\gamma\rangle$ of the stretching rate of material lines in two dimensions. Solid curve, $\langle\langle\gamma\rangle\rangle$, which is independent of the initial length $\ell(0)$ as seen in figure 8; thick dotted curve, $\langle\gamma\rangle$ for $\ell(0)=100\eta$; thin dotted curve, $\langle\gamma\rangle$ for $\ell(0)=10\eta$; dashed curve, $\langle\gamma\rangle$ for $\ell(0)=\eta$. Run IIC. Observe that $\langle\gamma\rangle$ approaches $\langle\langle\gamma\rangle\rangle$ as $\ell(0)$ increases.

It is also observed in figure 9 that the non-weighted average $\langle\gamma\rangle$ is larger for longer initial length $\ell(0)$ for the duration shown in this figure ($t \lesssim 40\tau_\eta$). This implies that, at a given Reynolds number, spatially more extended lines have a larger mean stretching rate $\langle\gamma\rangle$ as long as $\langle\delta\rangle < \mathscr{L}$. Note that mean extent $\langle\delta\rangle$ grows only algebraically (see figure 16*a* below). Incidentally, $\langle\gamma\rangle$ should tend to a unique value, i.e. Γ_∞, irrespective of the initial condition as t goes to infinity because all the tracked lines eventually become sufficiently long and extended.

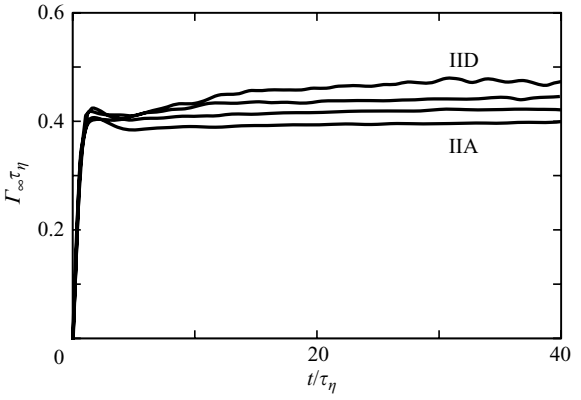

FIGURE 10. Average stretching rate Γ_∞ of sufficiently extended lines in two dimensions for four different Reynolds numbers.

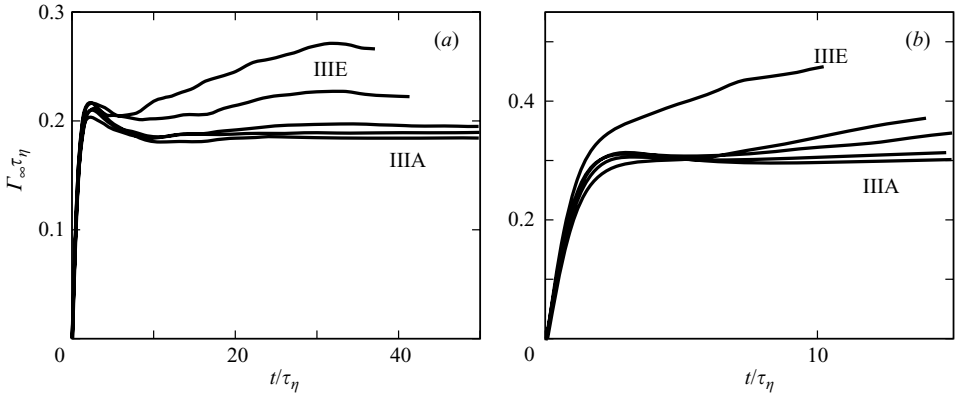

FIGURE 11. Weighted average of stretching rate (*a*) of lines and (*b*) of surfaces in three-dimensional turbulence for five different Reynolds numbers.

The temporal evolution of $\Gamma_\infty(t)$ for different Reynolds numbers in a two-dimensional DNS is plotted in figure 10. It starts at zero because of the random orientations of material lines at the initial instant, and increases rapidly within several τ_η (during this transient time a bump is observed in the graph, which is explained by Girimaji & Pope (1990) as an effect of vorticity on the material elements). Then it increases approximately linearly for the duration of the integral time $\mathscr{T}$ ($10\tau_\eta \sim 25\tau_\eta$), and probably tends to a value which increases with the Reynolds number. This Reynolds-number dependence of $\Gamma_\infty(t)\tau_\eta$ may be surprising given the observation that material line deformation is governed by eddies of the Kolmogorov scale (figure 7), but it is explained in the next section.

Similar behaviours are observed in the temporal evolutions of $\Gamma_\infty(t)$ of material lines and surfaces in three-dimensional turbulence as shown in figure 11. In the line simulation, we track an initially straight line with length $2\pi(\approx 2\mathscr{L})$, and repeat the simulation $M = 131$ (IIIA), 181 (IIIB), 35 (IIIC), 20 (IIID) and 20 (IIIE) times. For the surface simulation, we track an initially flat square surface with area of $(200\eta)^2$, and repeat it $M = 190$ (IIIA), 200 (IIIB), 135 (IIIC), 40 (IIID) and 32 (IIIE) times. Compared to the two-dimensional DNS (figure 10), the variation is large, probably because of the smallness of the number of tracked material objects. In particular, the

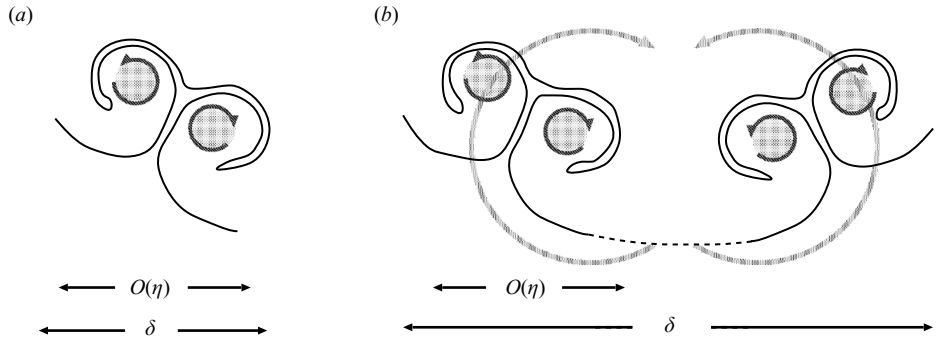

FIGURE 12. Schematic of folding by coherent eddies at a given Reynolds number for two different spatial extents δ of a material line. (*a*) For δ of $O(\eta)$, only Kolmogorov-scale eddies contribute the folding. (*b*) A more spatially extended line can be folded by many eddies of different scales between η and δ. The numerical evidence for this picture is given in movie 3 (in the online supplement), where the temporal evolution of a material line in two dimensions is visualized together with coarse-grained vorticity magnitude.

estimated large value for run IIIE might be accidental (note that M is only $O(10)$). Nevertheless, the trend is clear that the normalized stretching rate $\Gamma_\infty(t)\tau_\eta$ increases with the Reynolds number.

4. Folding effects as an origin of the Reynolds-number dependence

4.1. *Qualitative argument*

To summarize the numerical results described in the preceding section, the mean stretching rate $\langle\gamma\rangle$ of material objects at a given Reynolds number increases with their spatial extent $\langle\delta\rangle$ as long as $\langle\delta\rangle < \mathscr{L}$ (figure 9), and the normalized mean stretching rate $\Gamma_\infty\tau_\eta$ of sufficiently extended objects (i.e. $\langle\delta\rangle \gg \mathscr{L}$) takes larger values for larger Reynolds numbers (figures 10 and 11).

The first key ingredient necessary for understanding the above numerical results is the fact that the folding is more intensive for material objects of larger extent. As stated in §2 with reference to figures 4 and 7, the folding is caused by coherent eddies of counter-rotating pairs of various scales. If the size of material objects is $O(\eta)$, the folding is brought about only by swirling motions of the smallest eddies (figure 12*a*). If, on the other hand, the material object spreads over many of the smallest eddies ($\delta > \eta$), then many pairs of counter-rotating eddies of the smallest size, which are accompanied by the folded parts of the object, may meet owing to advection by larger eddies, leading to enhancement of folding (figure 12*b*). It should be noted here that this advection effect is brought about by all the eddies smaller than the extent δ of the material objects but not by those larger than it. Therefore the degree of folding is characterized by and increases with the ratio δ/η as long as δ is smaller than the integral scale $\mathscr{L}$, which is the maximal length scale of the constituent eddies of turbulence. For those material object extended more than $\mathscr{L}$ the degree of folding may be a function of $\mathscr{L}/\eta$, which increases with the Reynolds number.

Note that mean extent $\langle\delta\rangle$ increases slowly in time as long as it is larger than the Kolmogorov length η. More precisely, since the growth of $\langle\delta\rangle$ is described by the relative diffusion (Richardson 1926), $\langle\delta\rangle$ is expected to be proportional to $t^{3/2}$ for $\eta \ll \langle\delta\rangle \ll \mathscr{L}$, and proportional to $t^{1/2}$ for $\langle\delta\rangle \gg \mathscr{L}$. On the other hand, the line length

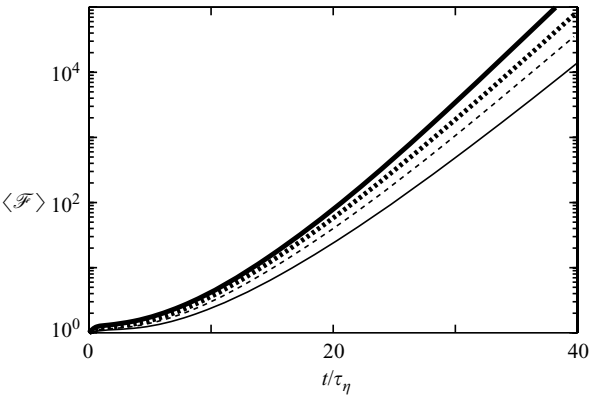

FIGURE 13. Average degree $\langle \mathscr{F} \rangle$ of folding of a sufficiently extended line ($\ell(0) = 100\eta$) in two dimensions for four different Reynolds numbers. Thin curve, run IIA; dashed curve, IIB; dotted curve, IIC; thick curve, IID.

$\ell(t)$ or the surface area $a(t)$ increases much faster, i.e. exponentially. This is because the stretching is predominantly caused by the Kolmogorov-scale eddies, whereas the growth of $\delta(t)$ is mainly due to eddies of scale $\delta(t)$. These two very different temporal evolutions of $\ell(t)$ (or $a(t)$) and $\delta(t)$ make the folded parts of a line (or a surface) accumulate in relatively small regions in space. This accumulation is, therefore, quite intensive and its effect cannot be neglected.

The second key ingredient is the fact that the folded parts of material objects accumulate non-uniformly in space and this non-uniformity increases the mean stretching rate because the degree of folding serves as the statistical weight. Because of the incompressibility of fluid, the accumulation is more intensive where the stretching is stronger (this may be obvious in the cases of lines in two dimensions and surfaces in three dimensions, and numerically confirmed in figures 14*b* and 18*a* below). Therefore, more strongly stretching parts can be more prominent in averaging by accumulation of folded lines or surfaces. This implies that the mean stretching rate of a material object significantly depends on the degree of folding.

Now we are ready to explain the Reynolds-number dependence of the mean stretching rate Γ_∞ of sufficiently extended material objects observed in figures 10 and 11. When $\delta > \mathscr{L}$, eddies of all length scales between η and $\mathscr{L}$ contribute to the folding of the material objects. Hence, at higher Reynolds numbers, eddies in a wider range of length scales contribute to folding, and therefore the degree of folding is larger. Consequently, the mean stretching rate, normalized by ${\tau_\eta}^{-1}$, may be larger for higher Reynolds number because strongly stretched parts are more emphasized by the intensive accumulation of folded objects.

This explanation is also consistent with the observation in figure 9 that initially longer lines have a larger stretching rate at a given Reynolds number. Since the lines considered in figure 9 are initially straight, longer lines have a larger extent. As lines with a larger extent are folded by a wider scale range of eddies (see figure 12), the folding is more intensive and the mean stretching rate becomes larger.

4.2. *Numerical verification 1: sufficiently extended lines*

A direct verification of the above physical explanation, in which the degree of folding is the key quantity, is given in figure 13, where we plot the mean multiplicity $\langle \mathscr{F} \rangle$ of

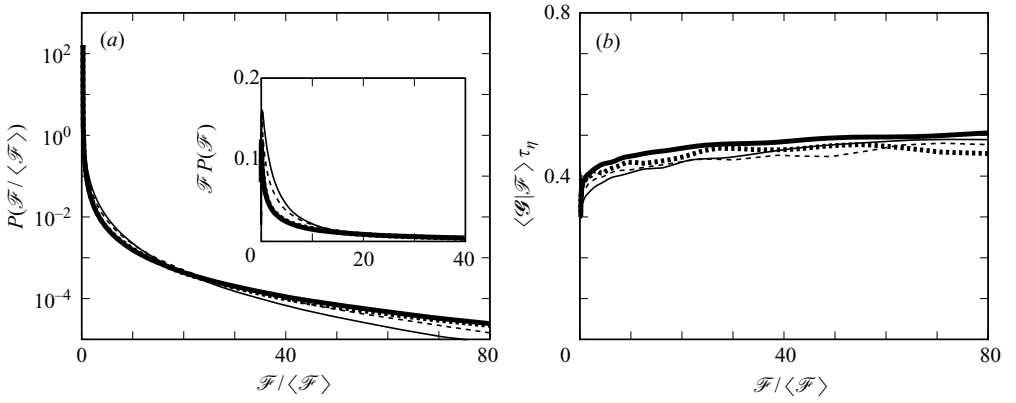

FIGURE 14. (*a*) PDF of $\mathscr{F}$. (*b*) Mean local stretching rate $\mathscr{G}$ conditioned by local degree $\mathscr{F}$ of folding. The inset in (*a*) shows the weighted PDF by $\mathscr{F}$. Thin curve, run IIA; dashed curve, IIB; dotted curve, IIC; thick curve, IID. $t = 40\tau_\eta$. $\ell(0) = 100\eta$.

folding of sufficiently extended lines ($\ell(0) = 100\eta$) in two dimensions for four different Reynolds numbers. Here, $\mathscr{F}$ is estimated by the number of overlapping material lines found in a small square with side length $\eta/20$, which is smaller than both the Kolmogorov length η and the numerical grid width. It is seen that $\langle\mathscr{F}\rangle$ increases exponentially with time and that the growth rate is larger for larger Reynolds numbers. This result is consistent with the qualitative observation in figure 7, and supports the argument in the preceding subsection that at a higher Reynolds number, the degree of folding is more intensive, and therefore the mean stretching rate is larger.

The above argument is strengthened by investigating the behaviour of the probability density function (PDF) $P(\mathscr{F})$ of the local degree $\mathscr{F}$ of folding and the conditional average $\langle\mathscr{G}|\mathscr{F}\rangle$ of local stretching rate $\mathscr{G}$ for a given $\mathscr{F}$. We plot, in figure 14, the PDF and the conditional average for material lines with initial length much longer than η (say, $\ell(0) = 100\eta$) at four different Reynolds numbers. The abscissa is the degree of folding normalized by its mean value. The PDF has a sharp peak at the origin and a long tail. Observe that the PDF tail is more extended for larger Reynolds numbers. This long tail may be due to the action of larger eddies (i.e. the long-time correlation of folding, see § 4.4). On the other hand, the conditional average is less dependent on the Reynolds number; the fluctuation in figure 14(*b*) is not small, but no monotonic dependence on the Reynolds number is observed for larger values of $\mathscr{F}$. It is also important that $\langle\mathscr{G}|\mathscr{F}\rangle$ is an increasing function of $\mathscr{F}$, as expected from the incompressibility of fluid, that is, the local stretching rate $\mathscr{G}$ and the folding $\mathscr{F}$ are positively correlated. The mean stretching rate is then calculated by

$$\Gamma_\infty = \frac{1}{\langle\mathscr{F}\rangle}\int_0^\infty \mathscr{F}\,\langle\mathscr{G}|\mathscr{F}\rangle\;P(\mathscr{F})\,\mathrm{d}\mathscr{F} \tag{4.1}$$

with $\langle\mathscr{F}\rangle = \int_0^\infty \mathscr{F}P(\mathscr{F})\,\mathrm{d}\mathscr{F}$. Note that Γ_∞ is expressed as a weighted average of $\langle\mathscr{G}|\mathscr{F}\rangle$ by $\mathscr{F}$. The fact that Γ_∞ depends on the Reynolds number (figure 10) implies that the tail of $P(\mathscr{F})$ contributes significantly to the integral in (4.1). More precisely, the inset in figure 14(*a*) shows that the contribution from the tail (say, $\mathscr{F}/\langle\mathscr{F}\rangle \gtrsim 20$) of $\mathscr{F}P(\mathscr{F}/\langle\mathscr{F}\rangle)$ to this integral cannot be neglected; note that in the range $\mathscr{F}/\langle\mathscr{F}\rangle \lesssim 20$ this function takes larger values for smaller Reynolds numbers, but the resultant integral is larger for larger Reynolds numbers.

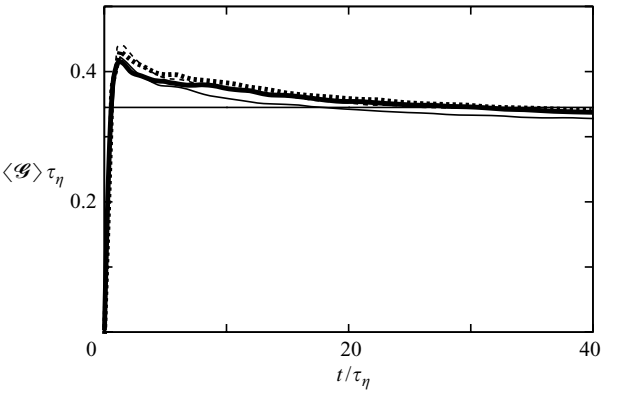

FIGURE 15. Stretching rate of material lines in two dimensions. Folded parts are artificially removed. Thin curve, run IIA; dashed curve, IIB; dotted curve, IIC; thick curve, IID. The horizontal straight line indicates 0.345, which corresponds to parameter g_1 in (4.5).

On the other hand, it is shown in figure 15 that the mean stretching rate

$$\langle \mathscr{G} \rangle = \int_0^\infty \langle \mathscr{G} | \mathscr{F} \rangle \, P(\mathscr{F}) \, \mathrm{d}\mathscr{F} \tag{4.2}$$

without the weighting by $\mathscr{F}$ does not depend on the Reynolds number. This artificial mean stretching rate $\langle \mathscr{G} \rangle$ corresponds to that where the multiplicity due to the folding of material lines is ignored and lines are treated as single ones. Comparing this figure with figure 10, it is clear that the folded parts contribute to the Reynolds-number dependence of Γ_∞. Incidentally, the saturated value of $\langle \mathscr{G} \rangle$ for a later stage of temporal evolution is about $0.345\tau_\eta^{-1}$, which turns out to agree with a model parameter developed in § 4.4.

4.3. *Numerical verification 2: lines with a given initial length in η units*

As explained in the preceding subsection, if the extent is different, then the degree of folding differs, and therefore the mean stretching rate is also different. Conversely, if both the extent $\langle \delta(0) \rangle$, in units of η, and the degree of folding $\langle \mathscr{F}(0) \rangle$ are the same at a given time $t = 0$, then $\langle \mathscr{F}(t) \rangle$ is the same at any time t (>0) when $\langle \delta(t) \rangle$ is smaller than $\mathscr{L}$, even if the Reynolds number is different. In such a case the stretching rate must be the same in Kolmogorov time units. This is demonstrated in figure 16 for the stretching rate of lines in two dimensions with the initial length $\ell(0) = \eta$. Here, we plot the temporal evolution of (*a*) mean line extent $\langle \delta \rangle$ and (*b*) the arithmetically averaged stretching rate $\langle \gamma \rangle$ for four different Reynolds numbers. The temporal evolution of $\langle \delta \rangle / \eta$ is independent of the Reynolds number, as expected from the viewpoint of relative diffusion in the inertial range of statistically self-similar turbulence (Richardson 1926). Recall that the initial length $\ell(0)$, and therefore the initial spatial extent $\delta(0)$, of the tracked lines are the same in units of Kolmogorov length η. Consequently, the temporal evolution of the non-weighted average $\langle \gamma \rangle$ of the stretching rate is also independent of the Reynolds number when $\langle \delta \rangle$ is within the inertial range.

Similar verification is performed for the case of lines in three dimensions, and is shown in figure 17. In these DNS, we track lines starting with a same initial length in Kolmogorov units, say $\ell(0) = 5\eta$, for five different Reynolds numbers. Similarly to the

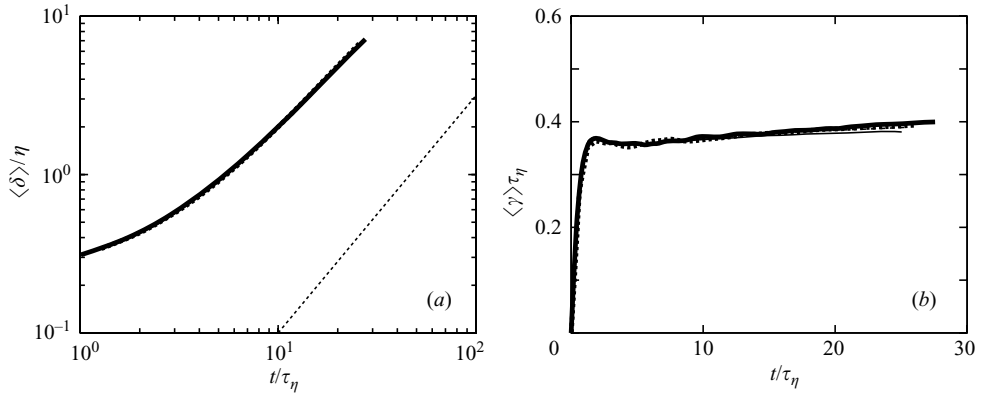

FIGURE 16. (*a*) Temporal evolution of the extent of material lines ($\ell(0)=\eta$) in two dimensions. Straight dotted line indicates $t^{3/2}$ corresponding to the Richardson diffusion. Thin curve, run IIA; dashed curve, IIB; dotted curve, IIC; thick curve, IID. (*b*) Arithmetically averaged stretching rate.

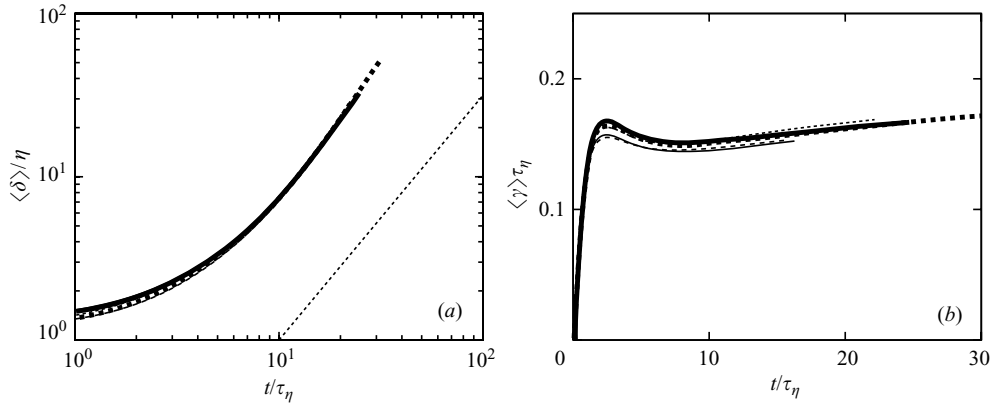

FIGURE 17. As figure 16 but for lines in three dimensions ($\ell(0)=5\eta$). (*a*) Average extent and (*b*) non-weighted average stretching rate. Straight line in (*a*) indicates the $t^{3/2}$ law. Thick curve, run IIIA; thick dashed curve, IIIB; dotted curve, IIIC; thin curve, IIID. thin dashed curve, IIIE.

above two-dimensional simulation, the temporal evolution of both of the mean extent $\langle\delta\rangle$ and non-weighted mean stretching rate is independent of the Reynolds number.

Although the above result that $\langle\gamma\rangle$ (see figures 16*b* and 17*b*) does not depend on the Reynolds number but $\langle\langle\gamma\rangle\rangle$ (see figures 10 and 11) does for lines starting with the same length in units of η may be perplexing, it can be explained as follows. Even if the temporal evolution of the mean extent $\langle\delta\rangle$ normalized by η does not depend on the Reynolds number (figures 16*a* and 17*a*), the tail of the PDF of δ expands more for larger Reynolds number cases (see figure 14 of Goto & Vassilicos 2004). Physically, the tail of the PDF of δ is explained as the effects of the action of larger eddies. Since, as seen in figure 9, the stretching rate is larger for more extended lines, well-extended lines contribute to the tail of the PDF of γ as well. Because of the existence of larger eddies in higher-Reynolds-number flow, some lines are extended very rapidly, folded intensively, and therefore have larger values of γ. Direct evidence for this statement is given in figure 18, where we plot (*a*) the average of γ conditioned by the degree $\mathscr{F}$

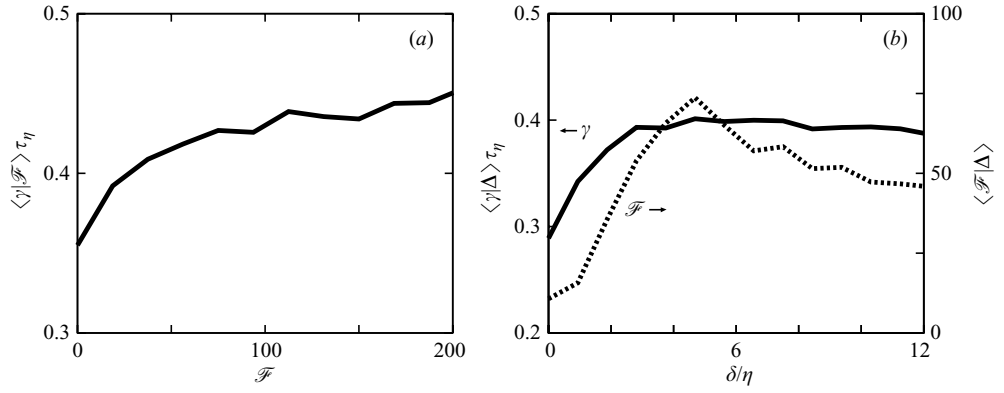

FIGURE 18. (a) Average of the stretching rate γ of material lines in two dimensions conditioned by the degree $\mathscr{F}$ of folding. $\ell(0)=\eta$, $t=25\tau_\eta$. Run IIC. (*b*) Conditional averages of γ (solid curve) and $\mathscr{F}$ on the extent Δ.

of folding, and (*b*) averages of γ and $\mathscr{F}$ conditioned by extent δ. These conditional averages are estimated over a large number of lines in a snapshot at a given time $t=25\tau_\eta$ with initial line length $\ell(0)=\eta$. We can see a very clear positive correlation between these three quantities in the region of δ/η smaller than 6, i.e. within the inertial range. Thus, even though there is no Reynolds-number dependence in $\langle\delta\rangle$ or $\langle\gamma\rangle$, the tails of their PDFs depend strongly on the Reynolds number. Accordingly, the average $\langle\langle\gamma\rangle\rangle$ weighted by ℓ depend on the Reynolds number because the weight $\ell\approx e^{\gamma t}$ emphasizes the tail of the PDF of γ.

4.4. *Quantitative argument*

Here, we develop a quantitative argument. As seen in figure 10, the stretching rate of sufficiently extended lines seems to saturate after a transient time of $O(\mathscr{T})$. These saturated values may be roughly estimated as follows. First, we assume, based on DNS observations, that coherent eddies of the Kolmogorov length survive for a sufficiently longer time than their turnover time (τ_η) and that their lifetime is of order of the integral time $\mathscr{T}$. Then, each eddy in a sufficiently extended material line can continue stretching it as long as the eddy survives. During the lifetime of an eddy, the total length of the stretched and accumulated material line around the eddy may be lengthened approximately by $\exp[\gamma_\eta\mathscr{T}]$ times. Here, γ_η is the stretching rate corresponding to the Kolmogorov-scale eddy. Therefore, the stretching rate Γ_∞ of a sufficiently extended material line may be roughly estimated as

$$\Gamma_\infty\approx\frac{\overline{\gamma_\eta\exp[\gamma_\eta\mathscr{T}]}}{\overline{\exp[\gamma_\eta\mathscr{T}]}}. \tag{4.3}$$

The overbar denotes the average over Kolmogorov eddies in the line tangle. If the distribution of stretching rate γ_η corresponding to Kolmogorov-scale eddies is assumed to be Gaussian, (4.3) reduces to

$$\Gamma_\infty\approx\overline{\gamma_\eta}+\overline{(\gamma_\eta-\overline{\gamma_\eta})^2}\mathscr{T}. \tag{4.4}$$

It might reasonably be assumed that both the average $\overline{\gamma_\eta}$ and variance $\overline{(\gamma_\eta-\overline{\gamma_\eta})^2}$ scale with τ_η^{-1} and τ_η^{-2} respectively because these are determined only by the statistical

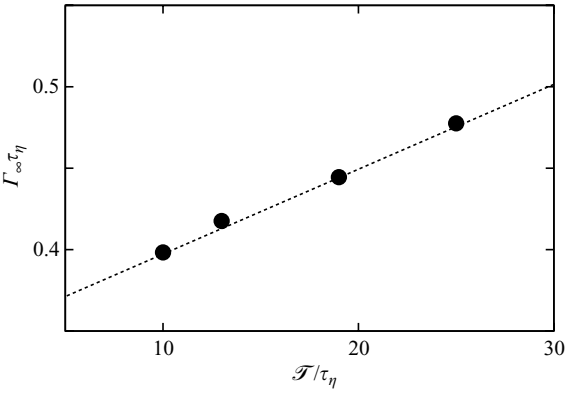

FIGURE 19. Saturated values of the stretching rate Γ_∞ of sufficiently extended lines in two dimensions. ●, DNS data estimated from the stationary period of figure 10; straight line, prediction (4.5) with $g_1 = 0.345$ and $g_2 = 0.00525$.

features of Kolmogorov-scale eddies. Thus, (4.4) leads to

$$\Gamma_\infty \tau_\eta \approx g_1 + g_2 \frac{\mathscr{T}}{\tau_\eta} . \tag{4.5}$$

Here, g_1 and g_2 are non-dimensional constants independent of the Reynolds number. We compare, in figure 19, prediction (4.5) with the numerical result. By choosing the constants as $g_1 = 0.345$ and $g_2 = 0.00525$, (4.5) can describe reasonably well the Reynolds-number dependence of Γ_∞ for lines in two dimensions. Notice that this value of $g_1 = 0.345$ approximately coincides with the saturated value of the mean stretching rate of the artificial simulation ignoring the multiplicity of folded parts shown in figure 15. This is expected from the construction of the above model because g_1 corresponds to the normalized stretching rate without folding.

For the three-dimensional cases, it is difficult to estimate accurately the saturated values of $\Gamma_\infty(t)$ for $t \gg \mathscr{T}$ from the DNS shown in figure 11 owing to large fluctuations and short integration times. However, noting the scaling $\mathscr{T}/\tau_\eta \sim R_\lambda$ in the three-dimensional isotropic turbulence, we may see that the Reynolds-number dependence observed in figure 11 seems much stronger than that expressed by (4.5). This may be due to the breakdown of the assumption of Gaussianity of the distribution of γ_η in three-dimensional isotropic turbulence. We have shown in Goto & Kida (2003) that the PDF of the infinitesimal-line-element stretching rate is not Gaussian and its tail gets longer as the Reynolds number increases.

5. Concluding remarks

We have shown in both two-dimensional and three-dimensional turbulence that the stretching rate Γ_∞, normalized by ${\tau_\eta}^{-1}$, of sufficiently extended lines or surfaces increases with the Reynolds number. The main cause of this Reynolds-number dependence is not linked to the development of the small-scale singularity in high-Reynolds-number turbulence. This is confirmed by the fact that the non-weighted arithmetic mean stretching rate of material line elements is independent of the Reynolds number† (see figure 20 for line elements in two dimensions, and Girimaji

† It is not known under which conditions the weighted mean stretching rate $\langle\langle\gamma\rangle\rangle$ of infinitesimal line or surface elements coincides with Γ_∞, although $\langle\langle\gamma\rangle\rangle$ equals Γ_∞ if the spatial distribution of

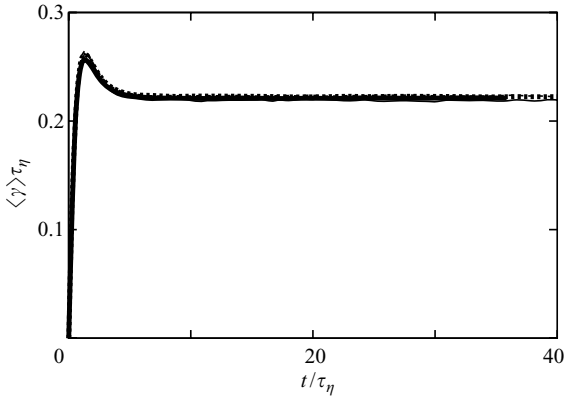

FIGURE 20. Non-weighted mean stretching rate $\langle\gamma\rangle$ of infinitesimal line elements in two dimensions. Thin curve, run IIA; dashed curve, IIB; dotted curve, IIC; thick curve, IID.

& Pope (1990) for line and surface elements in three dimensions). Note that if the reported Reynolds-number dependence were concerned with the development of the small-scale singularity, the statistics of infinitesimal elements would also depend on the Reynolds number.

The main cause of the Reynolds-number dependence stems from the accumulation and pile-up, around Kolmogorov-scale eddies, of material objects folded by eddies of various length scales. This accumulation of folded objects is spatially non-uniform and it is more intensive in stronger stretching regions. Therefore, it affects the mean stretching rate as the statistical weight. Since the folding of material objects can be described as a multiplicative process, this positive correlation between folding degree and stretching rate does not decay in time, and therefore the Reynolds-number dependence survives even after a sufficiently long time. Recall that this non-decaying correlation is an important contra-intuitive feature of multiplicative processes in contrast to additive ones (Goto & Kida 2002).

As mentioned at the beginning of the introduction, the study of material object deformation in turbulence is motivated by the desire to understand and control turbulent mixing. In this article, we have shed light on the folding of material objects for the first time, and have drawn the conclusion that the mean stretching rate of material objects is affected significantly by their folding property. Specifically, $\Gamma_\infty\tau_\eta$ is larger in larger-Reynolds-number flows as the folding is more intensive. This conclusion implies stronger mixing at larger Reynolds numbers because the strong stretching means an effective expansion of the boundary between subregions of fluid. It is also consistent with the intuitive picture that at larger Reynolds numbers, eddies in the wider range of length scales simultaneously fold the boundary between subregions to produce strong mixing of them. This article emphasizes that not only stretching but also folding of material objects must be considered to understand and control turbulent mixing.

This research is supported by Grant-in-Aid for Young Scientists from the Ministry of Education, Culture, Sports, Science and Technology.

material elements is infinitely dense. The argument in Sec.IIIF of Kida & Goto (2002) could be premature.

REFERENCES

Batchelor, G. K. 1952 The effect of homogeneous turbulence on material lines and surfaces. *Proc. Roy. Soc. London A* **213**, 349–366.

Batchelor, G. K. 1969 Computation of the energy spectrum in two-dimensional turbulence. *Phys. Fluids Suppl. II* **12**, 233–239.

Childress, S. & Gilbert, A. D. 1995 *Stretch, Twist, Fold: The Fast Dynamo*. Springer.

Cocke, W. J. 1969 Turbulent hydrodynamic line stretching: Consequences of isotropy. *Phys. Fluids* **12**, 2488–2492.

Frisch, U. & Vergassola, M. 1991 A prediction of the multifractal model—the intermediate dissipation range. *Europhys. Lett.* **14** 439–444.

Girimaji, S. S. & Pope, S. B. 1990 Material-element deformation in isotropic turbulence. *J. Fluid Mech.* **220**, 427–458.

Goto, S. & Kida, S. 2002 Multiplicative process of material line stretching by turbulence. *J. Turbulence* **3**, 017.

Goto, S. & Kida, S. 2003 Enhanced stretching of material lines by antiparallel vortex pairs in turbulence. *Fluid Dyn. Res.* **33**, 403–431.

Goto, S. & Vassilicos, J. C. 2004 Particle pair diffusion and persistent streamline topology in two-dimensional turbulence. *New J. Phys.* **6**, 65.

Guala, M., Lüthi, B., Liberzon, A., Tsinober, A. & Kinzelbach, W. 2005 On the evolution of material lines and vorticity in homogeneous turbulence. *J. Fluid Mech.* **533**, 339–359.

Huang, M.-J. 1996 Correlations of vorticity and material line elements with strain in decaying turbulence. *Phys. Fluids* **8**, 2203–2214.

Kida, S. & Goto, S. 2002 Line statistics: Stretching rate of passive lines in turbulence. *Phys. Fluids* **14**, 352–361.

Kraichnan, R. 1967 Inertial ranges in two-dimensional turbulence. *Phys. Fluids* **10**, 1417–1423.

Leith, C. E. 1968 Diffusion approximation for two-dimensional turbulence. *Phys. Fluids* **11**, 671–673.

Richardson, L. 1926 Atmospheric diffusion shown on a distance-neighbour graph. *Proc. Roy. Soc. Lond.* A **110**, 709–737.

Yakhot, V. & Sreenivasan, K. R. 2005 Anomalous scaling of structure functions and dynamic. *J. Statist. Phys.* **121**, 823–841.